In vitro pigmentation of human iPSC-derived retinal pigment epithelium cells does not indicate their quality for cell transplantation

Yoko Nakai-Futatsugi[1,2,3], Jianshi Jin[4+], Taisaku Ogawa[4], Noriko Sakai[1,2], Akiko Maeda[1,3,5], Ken-ichi Hironaka[6], Masakazu Fukuda[6], Hiroki Danno[6], Yuji Tanaka[1], Seiji Hori[2], Katsuyuki Shiroguchi[4], Masayo Takahashi[1,3,5,7*]

1. Laboratory for Retinal Regeneration, RIKEN Biosystems Dynamics Research (BDR), Kobe, Japan.
2. VC Cell Therapy Inc., Kobe, Japan.
3. Ritsumeikan University, Shiga, Japan.
4. Laboratory for Prediction of Cell Systems Dynamics, RIKEN Center for Biosystems Dynamics Research (BDR), Osaka, Japan.
5. Kobe City Eye Hospital, Department of Ophthalmology, Kobe, Japan.
6. Knowledge Palette, Inc., Kanagawa, Japan.
7. Vision Care, Inc., Kobe, Japan.

+Current address: State Key Laboratory of Integrated Management of Pest Insects and Rodents, Institute of Zoology, Chinese Academy of Sciences, Beijing, 100101, P. R. China.

*Correspondence: Masayo Takahashi (takahashi@vision-care.jp)

Key words: retinal pigment epithelium (RPE) cell; Automated Live imaging and cell Picking System (ALPS); single cell RNA sequencing; cell transplantation; quality management.

Abstract

Retinal pigment epithelium (RPE) cells show heterogeneous level of pigmentation when cultured *in vitro*. To know whether their color in appearance indicates functional qualities of the RPE, especially in terms of clinical use for cell transplantation, we analyzed the correlation between the color intensities and the gene expression profile of human-induced pluripotent stem cell-derived RPE cells (iPSC-RPE) at single cell level. For this purpose, we utilized our recent invention, Automated Live imaging and cell Picking System (ALPS), which enabled photographing each cell before RNA-sequencing analysis to profile the gene expression of each cell. While our iPSC-RPE were categorized in 4 clusters by gene expression, the color intensity of iPSC-RPE did not project any specific gene expression profiles, suggesting the degree of pigmentation of iPSC-RPE *in vitro* does not specifically correlate with quality metrics for clinical use.

Introduction

Retinal pigment epithelium (RPE) is a layer of cells paved by hexagonal, brown pigmented cells, which locates between the neural retina and the choroid. RPE cells play an important role in maintaining the visual system by supplying nutrition to the photoreceptors, phagocytosing mature outer segments of the photoreceptors, facilitating visual/retinoid cycle to produce a photosensitive derivative of vitamin A, absorbing stray light for the vision, and secreting vascular endothelial growth factor (VEGF) for the maintenance of choroid blood vessels (Kim et al., 2013; Lehmann et al., 2014; Lin et al., 2022). Abnormalities in the RPE cause a wide variety of retinal degenerative diseases such as age-related macular degeneration (AMD) which is a devastating disease leading to blindness. Medication for AMD is limited, and there are increasing attention on cell transplantation of RPE for the treatment. RPE transplantation for AMD to replace degenerated RPE with fetal RPE was introduced almost 3 decades ago (Algvere et al., 1994). Later, transplantation of autologous peripheral RPE to the degenerated site has also been reported (Binder et al., 2002). Our laboratory has pioneered in the production of RPE cells from human induced pluripotent stem cells (iPSC) and ocular transplantation of iPSC-derived RPE cells (iPSC-RPE) to replace degenerated RPE of AMD patients (Mandai et al. 2017; Sugita et al. 2020). For the quality management of iPSC-RPE transplants, we routinely verify the expressions of key factors such as *RPE65*, *Bestrophin*, *CRALBP* and *MERTK* by quantitative PCR; PAX6 and microphthalmia transcription factor (MiTF) by immunostaining; and pigment epithelium derived factor glycoprotein (PEDF) and VEGF by enzyme linked immunosorbent assay (ELISA). The morphology and pigmentation are also qualitatively checked, but there has been no means to link these appearances with gene expression.

Our recent invention, Automated Live imaging and cell Picking System (ALPS), enables the characterization of a cell that is actually showing a behavior of interest (Jin et al., 2023). While monitoring the cells in live, ALPS enables to pick up one single cell for further manipulation. In the present study, we utilized this system to monitor the color of iPSC-RPE cells, then to pick up one of the cells, followed by RNA-sequencing analysis to profile the gene expression of that single cell. In this way, we confirmed the iPSC-RPE cells that passed our quality management criteria for clinical use did not show strong correlation between the color and the expression of a specific gene, suggesting the degree of pigmentation in an iPSC-RPE cell do not indicate the functional quality of an RPE cell, in terms of the use as an RPE-transplant.

Results

ALPS enabled photographing each cell before RNA extraction

iPSC-RPE cells were produced from two human iPSC-lines of the Center for iPS Cell Research and Application (CiRA; iPSC-lines 201B7 and 253G1). The quality of the iPSC-RPE cells as RPE-transplants were verified by the expressions of *RPE65*, *Bestrophin*, *CRALBP* and *MERTK* by quantitative PCR; PAX6, MiTF and Bestrophin by immunostaining; and PEDF and VEGF by ELISA. Hexagonal morphologies and sufficient degree of pigmentation were also confirmed qualitatively (**Figure 1A**). Normally the degree of pigmentation of RPE cells increases during the culture period, culminating when the cells become confluent, and returns less pigmented when they are replated at sparse density. It is also normal that even at the most confluent state, RPE cells show diverse degree of pigmentation (**Figure 1A**). To characterize the cells with different degrees of pigmentation, 2034 cells of iPSC-RPE (96 cells each from 2 different dishes of 12 independent cultures of iPSC201B7-RPE and iPSC253G1-RPE cultured for 6 and 12 weeks; **Figure 1 -table 1**) were picked as single cells by ALPS and photographed under a light microscope (**Figure 1B** photos). The intensities of red, green and blue channels were measured for each cell (**Figure 1B** plots). Because of the strong correlation ($r > 0.99$) between the three channels (**Figure 1 -figure supplement 1**), we used the intensity of the blue channel, or the average intensity of the three channels (so-called brightness), as a proxy for color intensity of each cell.

Dark or white iPSC-RPE cells did not form a specific cluster by single cell transcriptome analysis

The iPSC-RPE cells picked by ALPS and photographed were then subjected to RNA-extraction followed by single cell RNA-sequencing analysis. To compare the gene expression profiles of our iPSC-RPE lines with other commercially available RPE cells, human fetal primary RPE cells purchased from Lonza were picked by ALPS after cultured for 6 and 12 weeks as well (**Figure1 -table 1**). The *t*-distributed stochastic neighbor embedding (*t*-SNE) plot of the transcriptomes of iPSC-RPE cells, Lonza-RPE cells together with undifferentiated human iPSCs and human fibroblasts showed our iPSC-RPE and Lonza-RPE in different clusters (**Figures 2A and B**). Although the parameters for *t*-SNE were adjusted to have all the iPSC-RPEs (iPSC201B7-RPE and iPSC253G1-RPE cultured for 6 and 12 weeks; **Figure1 -table 1**) mingle regardless of the original iPSC-line or the culture period (**Figure 2A**), our iPSC-RPE was divided in 4 sub-clusters (**Figure 2B**). The major 2 clusters (cluster-0 and -1) did not show critical

differences in the expressions of key factors for quality management (**Figure 2 -figure supplement 1**) or the gene-ontology terms (**Figure 2 -figure supplement 2**). Interestingly, cluster-8 that consisted of 32 cells showed the expression of proliferation marker *MKI67* which was not expressed in other clusters besides cluster-4 that represented iPSC (**Figure 2 -figure supplement 3**). Unlike iPSCs in cluster-4, the iPSC-RPE cells of cluster-8 did not show the expression of an iPSC-marker *LIN28A* (**Figure 2 -figure supplement 3**) denying the possibility of cluster-8 being a residual of iPSCs after RPE differentiation. It could be possible that cluster-8 implies the existence of adult stem cell population of RPE.

When the *t*-SNE plot was displayed with the color intensity of each cell, either deeply or lightly pigmented cells did not localize to a particular cluster (**Figure 2C**). Violin plots quantifying color intensities of the cells in each cluster showed all clusters having both dark- and light-colored cells (**Figure 2D**). Interestingly, Lonza-RPE showed biased distribution of cell-color among the 3 clusters (cluster-2, -3, and -7), having highly pigmented cells in cluster-2 and -3 but not in -7 (**Figure 2C and D**). These results indicated the degree of pigmentation of our iPSC-RPE did not associate with a specific gene expression profile defined by *t*-SNE.

There was no strong correlation between the color of iPSC-RPE and the gene expression

As no correlation between the color and gene expression profile was revealed in our iPSC-RPE by clustering analysis, next we sought the correlation of individual genes with the color of the cells. When each of the 28047 genes was analyzed for the correlation coefficient between its expression level and the color intensity in each cell, even for the gene with the highest positive- or negative-correlation with the color, the coefficient was 0.565 and -0.445, respectively (**Figure 3**). The gene with the highest correlation was *CST3* (correlation coefficient 0.565) that encodes cystatin C, a cysteine-proteinase inhibitor. As melanin, the material of the color, is cysteine-rich (D'Alba and Shawkey, 2019), it is reasonable to have increased level of melanin under upregulated *CST3* that inhibits cysteine-targeted degradation.

Intriguingly, the expressions of the genes directly related to the production of melanin were not the highest for the correlation with the color. For example, correlation coefficients between the expressions of the enzymes for melanin-synthesis, *TYR* and *TYRP1*, and color intensities were 0.434 and 0.458, respectively (**Figure 3A**). In other words, the darkest cells were not necessarily expressing the highest level of *TYR* or *TYRP1* mRNAs. This suggests the degree of pigmentation is dynamically regulated in

each cell, and there is a time-lag between mRNA expression, production of the enzymes and synthesis of melanin (descriptive image in **Figure 3 -figure supplement 1**).

Biological aspects that correlated with pigmentation of iPSC-RPE

Having the results suggesting the color of iPSC-RPE may not be an indicator of the expression levels of any of the critical genes used for quality management (**Figure 2 -figure supplement 1**), next we sought then which biological aspects underlie the degree of pigmentation of *in vitro* cultured iPSC-RPE cells. For this purpose, we re-analyzed the transcriptome of our iPSC-RPE cells shown in **Figure 1A**. First, we calculated the weighted sum of the RGB channels, the so-called brightness, and used it as a proxy for the pigmentation level. Then, by gene set enrichment analysis (GSEA) (Korotkevich et al., 2021), we identified 15 biological pathways, including lysosome- and complement-related pathways, enriched in darker cells, regardless of cell lineage (Lonza-RPE, iPS201-RPE, and iPS253-RPE) (**Figure 4**). Among lysosome-related genes, *PASP* and *CTSD* correlated with the color intensity of the cells at correlation coefficients 0.34 and 0.31, respectively (**Figure 4-figure supplement 1**). Among complement-related genes, *C1R, C1S* and *C3* correlated with the color intensity of the cells at correlation coefficients 0.31, 0.31 and 0.27, respectively (**Figure 4-figure supplement 2**). This correlation was partially consistent with the analysis of independent genes (**Figure 3**), which showed complement related genes *C1R, C1QTNF5* and *C1S*, and lysosome related gene *CTSD* within the top 20 of the genes that had positive correlation with color intensity (**Figure 3A** list on the right).

Gene set related to retinoid recycling, an important feature of the RPE to supply the photoreceptor with retinal, showed weak correlation with the color intensity of iPSC-RPE cells with correlation coefficients of genes such as *RDH11, BCO1, RDH10, DHRS3,* and *RDH5* at 0.25, 0.20, 0.16, 0.12 and 0.11, respectively (**Figure 4 -figure supplement 3**). The gene set related to melanin-synthesis, including the genes such as *DCT*, *TYRP1* and *TYR*, only showed weak correlation with the color intensity of iPSC-RPE (**Figure 4 -figure supplement 4**), which was consistent with the analysis of *TYRP1* and *TYR* shown in **Figure 3.**

Discussion

In this study, we showed the degree of pigmentation of *in vitro* cultured iPSC-RPE cells did not project specific gene ontological clusters, although it correlated to some extent with the expressions of complement- and lysosome-related genes. Eye,

as well as brain and testis, is an immune privilege organ, where inflammation by the immune system is minimized (Zhou et al. 2010; Chen et al. 2019; Mohan et al. 2022). To protect the photoreceptors from pathogens at this immune suppressive environment, RPE has an immune cell-like aspect with the capability of complement activation (Kunchithapautham et al., 2014; Chen et al. 2019; Jensen et al., 2020; Li et al., 2020; Schäfer et al., 2020) and phagocytosis (Boulton, 2014; Lehmann et al., 2014).

Besides these immunogenic aspects, pigmentation also confers protective function on RPE from different biological aspects. The material of the dark pigments, melanin, is conserved from bacteria to mammals, with diverse protective functions against damaging ultraviolet (UV) rays, free radicals, or toxins (D'Alba and Shawkey, 2019). In most species, melanin pigments are confined in an intracellular organelle called melanosome. In the eye, melanosomes locate in RPE cells and choroidal melanocytes, where they shield the photoreceptor to reduce backscattered light and remove free radicals (Boulton, 2014; Lehmann et al., 2014; D'Alba and Shawkey, 2019). Unlike skin melanin that is constantly synthesized in epidermal melanocytes, melanin in RPE cells decrease with age, making the retina vulnerable with less protection by the RPE. Several attempts were made to re-pigment RPE cells by supplying with melanosomes isolated from *ex vivo* RPE cells (Boulton, 2014) or more recently with artificial melanin-like nanoparticles (Kwon et al., 2022). In accordance with decreased amount of melanin in adult RPE, primary cultured adult RPE cells are less pigmented (Boulton, 2014). On the other hand, primary culture of fetal-derived RPE cells, although less pigmented initially, become heavily pigmented when confluent monolayers are formed (Maminishkis et al. 2006), reflecting the nature of melanosomes produced during a limited time window of embryogenesis (Boulton, 2014). More importantly, human embryonic stem cell (ESC)- or iPSC- derived RPE cells exhibit pigmentation when they become confluent (Boulton, 2014; Kamao et al., 2014) suggesting these cells may retain or have been reprogrammed to gain the characteristics of fetal RPE cells. The Lonza-RPE cells (line #476621) used in this study were fetal-derived. Our iPSC-RPE formed different clusters from Lonza-RPE by single cell transcriptome analysis, which was consistent with our previous study showing the gene expression pattern of our iPSC-RPE was slightly different from Lonza-RPE, although it was closer than human RPE cell-line ARPE19, (Kamao et al., 2014). Interestingly, the pigmentation level of Lonza-RPE cells correlated with their gene expression profile (**Figure 2D**), which may be reflecting the developmental process of RPE that gains protective function, including melanogenesis, during embryogenesis. From this aspect, ESC- or iPSC-derived RPE cells may be more plastic, retaining immature profiles

although apparently being pigmented spontaneously. In fact, there are several lines of evidence implying *in vitro* pigmentation of stem cell-derived RPE cells may not necessarily reflect their levels of functional maturation. For example, bone marrow-derived RPE cells that are poorly pigmented *in vitro* become highly pigmented when transplanted (Sengupta et al., 2009), as well as our iPSC-RPE cells that are not pigmented when prepared but actually become heavily pigmented after engrafted (Mandai et al., 2017; Sugita et al., 2020), suggest the significance of environmental niche for melanogenesis. When stem cell-derived RPE cells are cultured *in vitro*, they are apparently not pigmented at sparse density, probably due to dilution amongst daughter cells (Boulton, 2014) or secretion of melanin by the fusion of melanosome membrane to the plasma membrane as proposed in melanocytes (Moreiras et al., 2021), but they become pigmented when they form a confluent monolayer, which is a reversible effect as the dynamics of pigmentation repeats when they are re-plated at a sparse density and become confluent again (**Figure 3 -figure supplement 1**). This again suggest the involvement of extracellular cues for pigmentation, besides the intrinsic characteristics of each RPE cell. Indeed, it has been shown that *in vitro* pigmentations of RPE cells are enhanced by extracellular matrix (Boulton, 2014) or even more intriguingly by phagocytosis of rod outer segments (Schraermeyer et al., 2006).

Without the exposure to pathogens or photoreceptor outer segments, *in vitro* pigmentation of iPSC-RPE cells could be somewhat a spontaneous but not a necessary sign to show they are prone to execute their protective function.

Materials and Methods

Cell culture

The study was approved by the ethical committees of the Institute of Biomedical Research and Innovation Hospital and the RIKEN Center for Developmental Biology, Japan. Human iPSC-lines 201B7 (HPS4290) and 253G1 (HPS0002) (Nakagawa et al., 2008) were provided by the RIKEN BRC through the National BioResource Project of the MEXT/AMED, Japan. iPSCs were cultured and differentiated into RPE cells as described previously (Kamao et al., 2014). Briefly, to differentiate human iPSCs into RPE cells, human iPSCs were cultured on gelatin-coated dishes in differentiation medium (GMEM (Sigma) supplemented with 1mM sodium pyruvate, 0.1 mM non-essential amino acids (Sigma), and 0.1 mM 2-mercaptoethanol (Sigma)) with 20% KnockOut Serum Replacement (KSR; Invitrogen) for four days, 15% KSR for six days, and 10% KSR for 20 days. Y-27632 (10 μM; Wako), SB431542 (5 μM; Sigma), and CKI7 (3 μM; Sigma) were added for the initial 18 days. After the emergence of pigmented cells, the medium was switched to SFRM (DMEM/F12 [7:3] supplemented with B27 (Invitrogen), 2 mM L-glutamine).

Lonza-RPE cells (line #476621; Lonza) were maintained in SFRM as well.

Human dermal fibroblasts were obtained from a healthy doner and cultured as described previously (Sugita et al., 2015).

Cell preparation for ALPS

Cell concentrations was measured using Hemocytometer Standard Specification (Improved Neubauer) (HIRSCHMANN LAB). 3 ml of PBS (D-PBS(-) without Ca and Mg, #14249-95, Nacalai Tesque Inc.) containing 0.25-1.0x10^4 cells were added onto a dish (PrimeSurface Dish 35, #MS-9035X, SUMITOMO BAKELITE CO, LTD.).

Imaging, isolation, and RNA-seq for single cells

Live cell imaging, cell picking, and single cell digital RNA-seq (Shiroguchi et al., 2012; Ogawa et al., 2017) were performed as described previously (Jin et al., 2023) except for the followings: In total, 4032 cells (**Figure 1 –table 1**) were measured and analyzed. Cell images (400 pixel × 330 pixel; 0.36 μm/pixel) were captured by both bright field and fluorescent channels (filter unit: mCherry C-FLL-C, Nikon Co.) with 20× objective (N.A. 0.7) and a color camera (Color Camera Nikon DS-Ri2, Nikon Co.). Exposure times for bright field and fluorescence were 10 ms and 100 ms, respectively. For both

channels, Z-stacks (21 planes) were recorded with 1-μm interval. Randomly selected cells were picked ("random selection" of ALPS (Jin et al., 2023)). For the picked single cells, library preparation including cell lysis, RNA fragmentation, cDNA generation with molecular barcode attachment, amplification, and purification was performed using the Bravo NGS workstation (Agilent Technologies) and thermal cyclers (Mastercycler X50s, Eppendorf). The libraries were mixed using different indexes, and sequenced on HiSeq (Illumina, 150 cycle) using custom primers. Detected number of RNA molecules for each gene in each cell was counted based on molecular barcodes.

All sequencing datasets have been deposited in the Genome Expression Omnibus database under accession No. GSE242184.

To estimate the RGB values of the cells within the cell images, first, the average intensities (0-255) per pixel for R, G, and B channels, respectively, of a circular area with a radius of 50 pixels at the position (195, 169 (coordinates in pixel)) of each cell image that covered the cell, and the area other than the circular area (background) were calculated. Then, for each image and each channel, the average intensity of the background was subtracted by the average intensity of the circular area. Finally, for each cell and each channel, the mean and standard deviation of the subtracted average circular area intensities of all 21 Z-stack images were obtained. The circular area images of iPSC-RPE cells are illustrated in Figure 1B.

Single cell transcriptome analysis

Single cell RNA-seq data were analyzed using Seurat v4 (Satija et al., 2015; Butler et al., 2018; Stuart et al., 2019; Hao et al., 2021) with R v4.2.1 (R Core Team (2022)). For cluster analyses in Figure 2, the following parameters were used:

FindNeighbors(dims = 1:6)
FindClusters(resolution = 0.4)
RunTSNE(all, dims = 1:6).

Brightness calculation

The brightness value Y for each cell was calculated by taking a weighted sum of the background-corrected intensities of the RGB channels (International Telecommunication Union, 2022):

$$Y = (0.299, 0.587, 0.114) \cdot (R_{\mathrm{corr}}, G_{\mathrm{corr}}, B_{\mathrm{corr}}),$$

where the background-corrected intensities of the RGB channels were obtained by

adding a virtual white background to delta intensities of RGB channels of each cell:

$$(R_{\mathrm{corr}}, G_{\mathrm{corr}}, B_{\mathrm{corr}}) = (255, 255, 255) + (\Delta R, \Delta G, \Delta B).$$

If the corrected intensity exceeded 255, it was replaced by the maximum value below 255 (there was only one such case). The resultant cellular brightness $Y \in [0,255]$ had a skewed distribution around the background brightness value, 255. Then, normalized brightness Y_{norm} was obtained by logit transformation, so that its range takes the entire real number.

$$Y_{\mathrm{norm}} = \log\left(\frac{Y}{255 - Y}\right)$$

The normalized brightness $Y_{\mathrm{norm}} \in [-\infty, \infty]$ was approximately normally distributed.

Pathway enrichment analysis

For each of the three RPE cell lineage (Lonza-RPE, iPS201-RPE, and iPS253-RPE), we explored biological pathways correlated with pigmentation levels according to the following steps:

1. Calculate Pearson's correlation coefficient between scaled gene expression levels ("scale.data" slot of a Seurat object) and the normalized brightness Y_{norm}.
2. Perform GSEA-preranked by the fgsea library in R using the gene list ranked by absolute value of Pearson's correlation coefficient as input and the KEGG pathway of MSigDB (c2.cp.kegg.v2023.1.Hs.symbols.gmt) as a reference (Liberzon et al., 2011; Korotkevich et al., 2021).
3. Define pathways with FDR<0.05 as significant (conventional criteria for GSEA).
4. Divide significant pathways into brightness-correlated pathways (NES>0) and -uncorrelated pathways (NES<0).

Finally, for each of the brightness-correlated and -uncorrelated significant pathways, we extracted the intersection, i.e., pathways commonly enriched in all three cell lineages. Note that although we found 15 common brightness-correlated pathways among three cell lines, no brightness-uncorrelated pathways were detected even in any of three cell lines.

References

Algvere PV, L Berglin, P Gouras, Y Sheng. Transplantation of fetal retinal pigment epithelium in age-related macular degeneration with subfoveal neovascularization. Graefes Arch Clin Exp Ophthalmol. 1994 232:707-716. doi:10.1007/BF00184273.

Binder S, Stolba U, Krebs I, Kellner L, Jahn C, Feichtinger H, Povelka M, Frohner U, Kruger A, Hilgers R-D, Krugluger W. Transplantation of autologous retinal pigment epithelium in eyes with foveal neovascularization resulting from age-related macular degeneration: a pilot study. Am J Ophthalmol 2002 133:215–225. doi:10.1016/s0002-9394(01)01373-3.

Boulton ME. Studying melanin and lipofuscin in RPE cell culture models. Exp Eye Res. 2014 126:61-67. doi:10.1016/j.exer.2014.01.016.

Butler A, Hoffman P, Smibert P, Papalexi E, Satija R. Integrating single-cell transcriptomic data across different conditions, technologies, and species. Nature Biotechnology 2018 36:411-420. doi:10.1038/nbt.4096.

Chen M, Luo C, Zhao J, Devarajan G, Xu H. Immune regulation in the aging retina. Prog Retin Eye Res 2019 69:159-172. doi: 10.1016/j.preteyeres.2018.10.003.

D'Alba L, Matthew D Shawkey. Melanosomes: Biogenesis, Properties, and Evolution of an Ancient Organelle. Physiol Rev. 2019 99:1-19. doi: 10.1152/physrev.00059.2017.

Hao Y, Hao S, Andersen-Nissen E, III WMM, Zheng S, Butler A, Lee MJ, Wilk AJ, Darby C, Zagar M, Hoffman P, Stoeckius M, Papalexi E, Mimitou EP, Jain J, Srivastava A, Stuart T, Fleming LB, Yeung B, Rogers AJ, McElrath JM, Blish CA, Gottardo R, Smibert P, Satija R. Integrated analysis of multimodal single-cell data. Cell 2021 doi:10.1016/j.cell.2021.04.048.

International Telecommunication Union. Updated 2022-7-27. https://www.itu.int/rec/R-REC-BT.601/

Jensen EG, Thomas Stax Jakobsen, Steffen Thiel, Anne Louise Askou, Thomas J Corydon. Associations between the Complement System and Choroidal Neovascularization in Wet Age-Related Macular Degeneration. Int J Mol Sci 2020

21:9752. doi: 10.3390/ijms21249752.

Jin J, Ogawa T, Hojo N, Kryukov K, Shimizu K, Ikawa T, Imanishi T, Okazaki T, Shiroguchi K. Robotic data acquisition with deep learning enables cell image-based prediction of transcriptomic phenotypes. Proc Natl Acad Sci U S A. 2023 120:e2210283120. doi: 10.1073/pnas.2210283120.

Kamao H, Mandai M, Okamoto S, Sakai N, Suga A, Sugita S, Kiryu J, Takahashi M. Characterization of Human Induced Pluripotent Stem Cell-Derived Retinal Pigment Epithelium Cell Sheets Aiming for Clinical Application. Stem Cell Reports 2014 2:205–218. https://doi.org/10.1016/j.stemcr.2013.12.007

Kim JY, Zhao H, Martinez J, Doggett TA, Kolesnikov AV, Tang PH, Ablonczy Z, Chan C-C, Zhou Z, Green DR, Ferguson TA. Noncanonical autophagy promotes the visual cycle. Cell 2013 154:365-376. doi:10.1016/j.cell.2013.06.012.

Korotkevich G, Sukhov V, Budin N, Shpak B, Artyomov MN, Sergushichev A. Fast gene set enrichment analysis. bioRxiv 2021 https://www.biorxiv.org/content/10.1101/060012v3

Kunchithapautham K, Carl Atkinson, Bärbel Rohrer. Smoke Exposure Causes Endoplasmic Reticulum Stress and Lipid Accumulation in Retinal Pigment Epithelium through Oxidative Stress and Complement Activation. J Biol Chem 2014 289:14534–14546. https://doi.org/10.1074/jbc.M114.564674

Kwon YS, Min Zheng, Alice Yang Zhang, Zongchao Han. Melanin-like Nanoparticles as an Alternative to Natural Melanin in Retinal Pigment Epithelium Cells and Their Therapeutic Effects against Age-Related Macular Degeneration. ACS Nano. 2022 16:19412-19422. doi:10.1021/acsnano.2c09087.

Lehmann GL, Ignacio Benedicto, Nancy J Philp, Enrique Rodriguez-Boulan. Plasma membrane protein polarity and trafficking in RPE cells: past, present and future. Exp Eye Res 2014 126:5-15. doi:10.1016/j.exer.2014.04.021.

Li XuanTan, Germera CJ, Nils La Cunza NL, AparnaLakkaraju A. Complement activation, lipid metabolism, and mitochondrial injury: Converging pathways in

421 age-related macular degeneration. Redox Biology 2020 37.
422 https://doi.org/10.1016/j.redox.2020.101781.
423
424 Liberzon A, Subramanian A, Pinchback R, Thorvaldsdóttir H, Tamayo P, Mesirov JP.
425 Molecular signatures database (MSigDB) 3.0 Bioinformatics 2011 27:1739–1740.
426 https://doi.org/10.1093/bioinformatics/btr260
427
428 Lin JB, Murakami Y, Miller JW, Vavvas DG. Neuroprotection for Age-Related Macular
429 Degeneration. Ophthalmol Sci 2022 2:100192. doi: 10.1016/j.xops.2022.100192.
430
431 Maminishkis A, Chen S, Jalickee S, Banzon T, Shi G, Wang FE, Ehalt T, Hammer JA,
432 Miller SS. Confluent Monolayers of Cultured Human Fetal Retinal Pigment Epithelium
433 Exhibit Morphology and Physiology of Native Tissue. Investigative Ophthalmology &
434 Visual Science 2006 47:3612-3624. https://doi.org/10.1167/iovs.05-1622
435
436 Mandai M, Watanabe A, Kurimoto Y, Hirami Y, Morinaga C, Daimon T, Fujihara M,
437 Akimaru H, Sakai N, Shibata Y, Terada M, Nomiya Y, Tanishima S, Nakamura M,
438 Kamao H, Sugita S, Onishi A, Ito T, Fujita K, Kawamata S, Go MJ, Shinohara C, Hata
439 KI, Sawada M, Yamamoto M, Ohta S, Ohara Y, Yoshida K, Kuwahara J, Kitano Y,
440 Amano N, Umekage M, Kitaoka F, Tanaka A, Okada C, Takasu N, Ogawa S, Yamanaka
441 S, Takahashi M. Autologous Induced Stem-Cell-Derived Retinal Cells for Macular
442 Degeneration. N Engl J Med 2017 376:1038-1046. doi: 10.1056/NEJMoa1608368
443
444 Mohan KV, Alaknanda Mishra, Abaranjitha Muniyasamy, Prakriti Sinha, Parul Sahu,
445 Ashwani Kesarwani, Kshama Jain, Perumal Nagarajan, Vinod Scaria, Manisha Agarwal,
446 Naseem S. Akhter, Chanda Gupta & Pramod Upadhyay. Immunological consequences
447 of compromised ocular immune privilege accelerate retinal degeneration in retinitis
448 pigmentosa. Orphanet Journal of Rare Diseases 2022 17:378.
449 https://doi.org/10.1186/s13023-022-02528-x
450
451 Moreiras H, Seabra MC, Barral DC. Melanin Transfer in the Epidermis: The Pursuit of
452 Skin Pigmentation Control Mechanisms. Int J Mol Sci 2021 22:4466.
453 https://doi.org/10.3390/ijms22094466
454
455 Nakagawa M, Koyanagi M, Tanabe K, Takahashi K, Ichisaka T, Aoi T, Okita K,
456 Mochiduki Y, Takizawa N, Yamanaka S. Generation of induced pluripotent stem cells

457 without Myc from mouse and human fibroblasts. Nat Biotechnol 2008 26:101-106.
458 doi:10.1038/nbt1374
459
460 Ogawa T, Kryukov K, Imanishi T, Shiroguchi K. The efficacy and further functional
461 advantages of random-base molecular barcodes for absolute and digital quantification of
462 nucleic acid molecules. Sci Rep 2017 7:13576. doi:10.1038/s41598-017-13529-3.
463
464 R Core Team (2022). R: A language and environment for statistical computing. R
465 Foundation for Statistical Computing, Vienna, Austria. URL https://www.R-project.org/.
466
467 Satija R, Farrell JA, Gennert D, Schier AF, Regev A. Spatial reconstruction of
468 single-cell gene expression data. Nature Biotechnology 2015 33:495-502.
469 doi:10.1038/nbt.3192, https://doi.org/10.1038/nbt.3192.
470
471 Schäfer N, Wolf HN, Enzbrenner A, Schikora J, Reichenthaler M, Enzmann V, Pauly D.
472 Properdin Modulates Complement Component Production in Stressed Human Primary
473 Retinal Pigment Epithelium Cells. Antioxidants 2020 9:793.
474 https://doi.org/10.3390/antiox9090793
475
476 Schraermeyer U, Kopitz J, Peters S, Henke-Fahle S, Blitgen-Heinecke P, Kokkinou D,
477 Schwarz T, Bartz-Schmidt KU. Tyrosinase biosynthesis in adult mammalian retinal
478 pigment epithelial cells. Experimental Eye Research 2006 83:315-321.
479 https://doi.org/10.1016/j.exer.2005.12.015
480
481 Sengupta N, Caballero S, Sullivan SM, Chang L-J, Afzal A, Calzi SL, Kielczewski JL,
482 Prabarakan S, Ellis EA, Moldovan L, Moldovan NI, Boulton ME, Grant MB, Scott EW,
483 Harris JR. Regulation of adult hematopoietic stem cells fate for enhanced tissue-specific
484 repair. Mol Ther 2009 17:1594-1604. doi:10.1038/mt.2009.145.
485
486 Shiroguchi K, Jia TZ, Sims PA, Xie XS. Digital RNA sequencing minimizes
487 sequence-dependent bias and amplification noise with optimized single-molecule
488 barcodes. Proc. Natl. Acad. Sci. USA 2012 109:1347-1352. doi:
489 10.1073/pnas.1118018109.
490
491 Stuart T, Butler A, Hoffman P, Hafemeister C, Papalexi E, III WMM, Hao Y, Stoeckius
492 M, Smibert P, Satija R. Comprehensive Integration of Single-Cell Data. Cell 2019

177:1888-1902. doi:10.1016/j.cell.2019.05.031

Sugita S, Kamao H, Iwasaki Y, Okamoto S, Hashiguchi T, Iseki K, Hayashi N, Mandai M, Takahashi M. Inhibition of T-cell activation by retinal pigment epithelial cells derived from induced pluripotent stem cells. Invest Ophthalmol Vis Sci 2015 56:1051-1062. doi: 10.1167/iovs.14-15619.

Sugita S, Mandai M, Hirami Y, Takagi S, Maeda T, Fujihara M, Matsuzaki M, Yamamoto M, Iseki K, Hayashi N, Hono A, Fujino S, Koide N, Sakai N, Shibata Y, Terada M, Nishida M, Dohi H, Nomura M, Amano N, Sakaguchi H, Hara C, Maruyama K, Daimon T, Igeta M, Oda T, Shirono U, Tozaki M, Totani K, Sugiyama S, Nishida K, Kurimoto Y, Takahashi M. HLA-Matched Allogeneic iPS Cells-Derived RPE Transplantation for Macular Degeneration. J Clin Med 2020 9:2217. doi: 10.3390/jcm9072217.

Zhou R, Caspi RR. Ocular immune privilege. F1000 Biol Rep 2010 2:3. doi: 10.3410/B2-3.

Figures

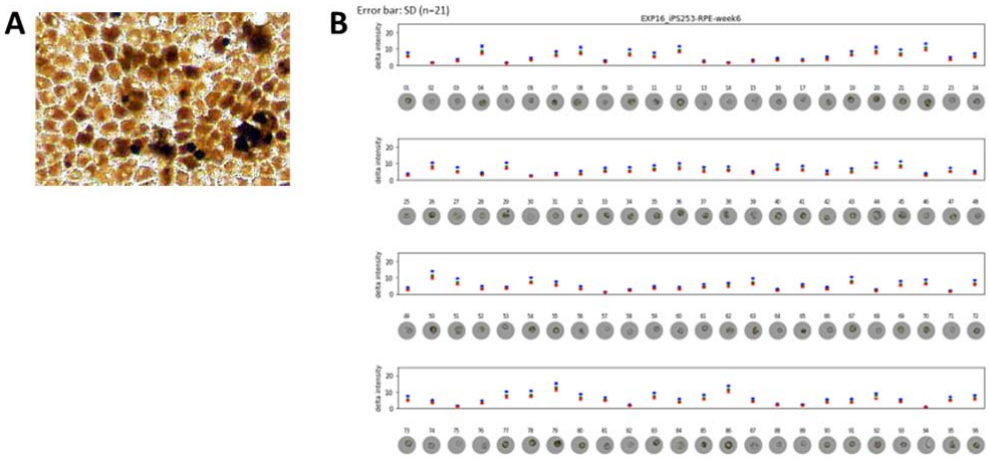

Figure 1 ALPS enabled photographing each cell before RNA extraction

A iPSC-RPE *in vitro* shows diverse degree of pigmentation among the cells. **B** Each cell was picked by ALPS and photographed under a light-microscope. The intensities of red, green and blue were measured. As there was no difference among the three intensities, the intensity of blue wavelength was used to represent the color intensity of each cell (see also **Figure 1 –figure supplement 1**).

523 **Figure 1 –table 1** The cells picked by ALPS and subjected to single cell
524 transcriptome analysis

iPS253-RPE	6W	192 cells (2plates)	x3 cultures
iPS201-RPE	6W	192 cells (2plates)	x3 cultures
Lonza-RPE	6W	192 cells (2plates)	x3 cultures
iPS253-RPE	12W	192 cells (2plates)	x3 cultures
iPS201-RPE	12W	192 cells (2plates)	x3 cultures
Lonza-RPE	12W	192 cells (2plates)	x3 cultures
iPS253		192 cells (2plates)	x1
iPS201		192 cells (2plates)	x1
Fibroblast		192 cells (2plates)	x1

525

526

527

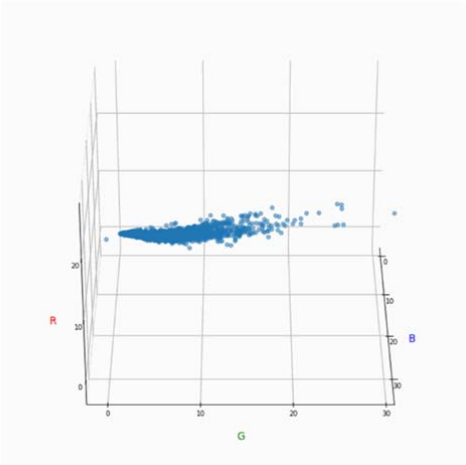

Figure 1 –figure supplement 1 Since the red-, green- and blue-intensities were linearly correlated among the iPSC-RPE cells, the intensity of blue wavelength was used to represent the color intensity of each cell in the following analyses.

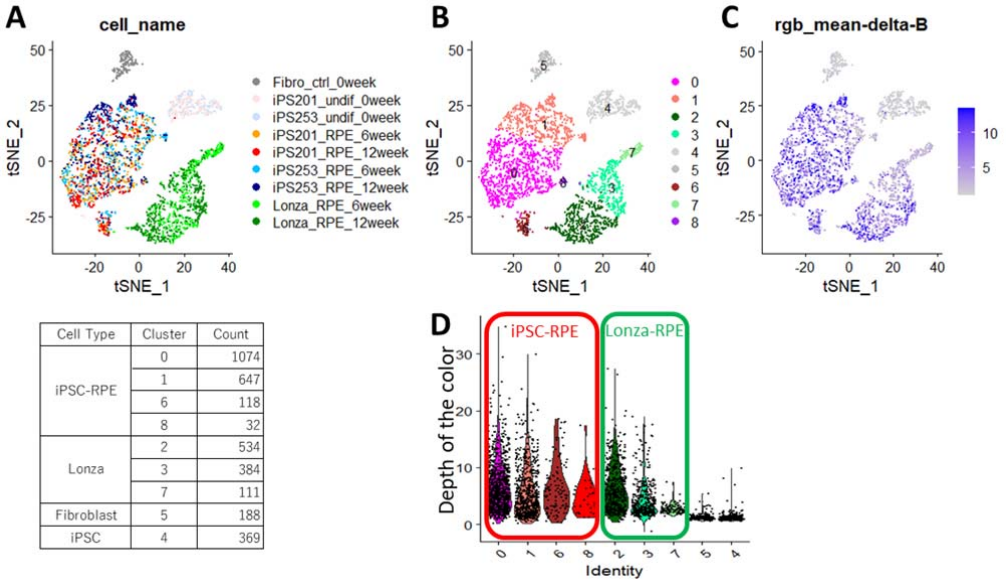

Cell Type	Cluster	Count
iPSC-RPE	0	1074
	1	647
	6	118
	8	32
Lonza	2	534
	3	384
	7	111
Fibroblast	5	188
iPSC	4	369

Figure 2 Single cell transcriptome analysis of the cells picked with ALPS.
Two-dimension plotting of the gene expression profile of each cell colored by the cell-types (**A**), clusters defined by gene expression profiles (**B**) or color intensities (**C**), and a violin plot quantitatively showing color intensities of the cells in each cluster **(D).** **A** iPSC-RPE cells formed a different cluster from Lonza-RPE. **B** iPSC-RPE cells were a heterogeneous population consisted of 4 sub-clusters. **C, D** Either very black or very white cells did not localize to a specific sub-cluster of iPSC-RPE.

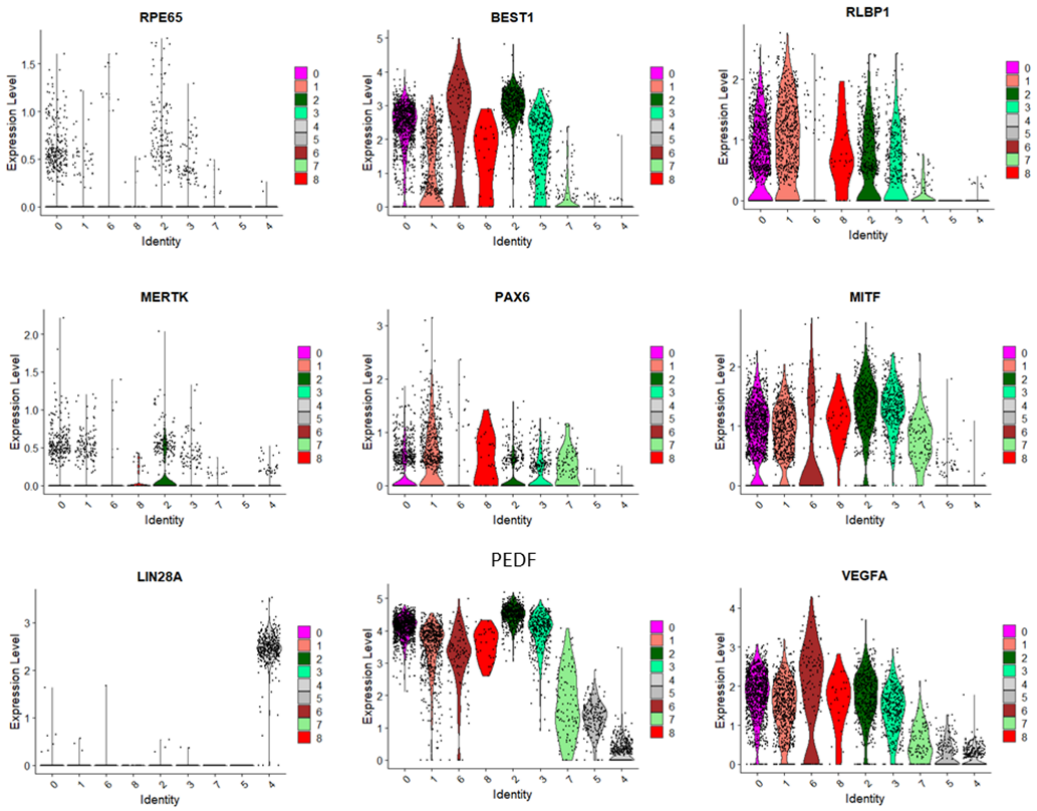

Figure 2 -figure supplement 1 The expression levels of the genes critical for quality management of iPSC-RPE cells for clinical use are shown by violin plots of each cluster defined in **Figure 2B**.

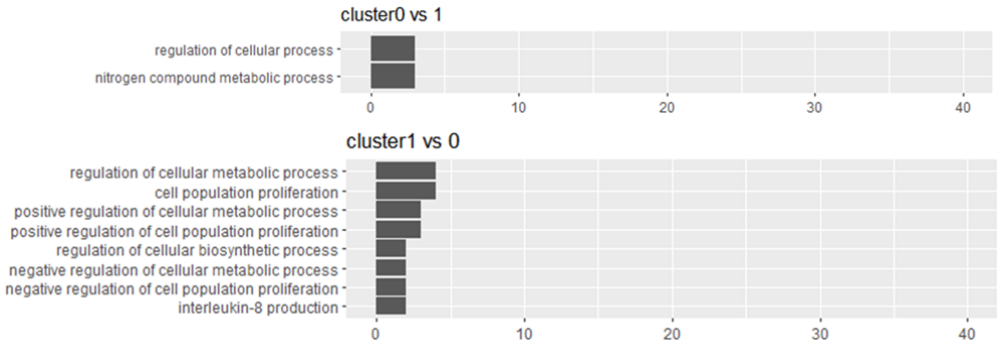

Figure 2 -figure supplement 2 Gene enrichment analysis of the 2 major clusters of iPSC-RPE (cluster 0 and 1) defined in **Figure 2B** did not elucidate qualitatively significant difference between the two.

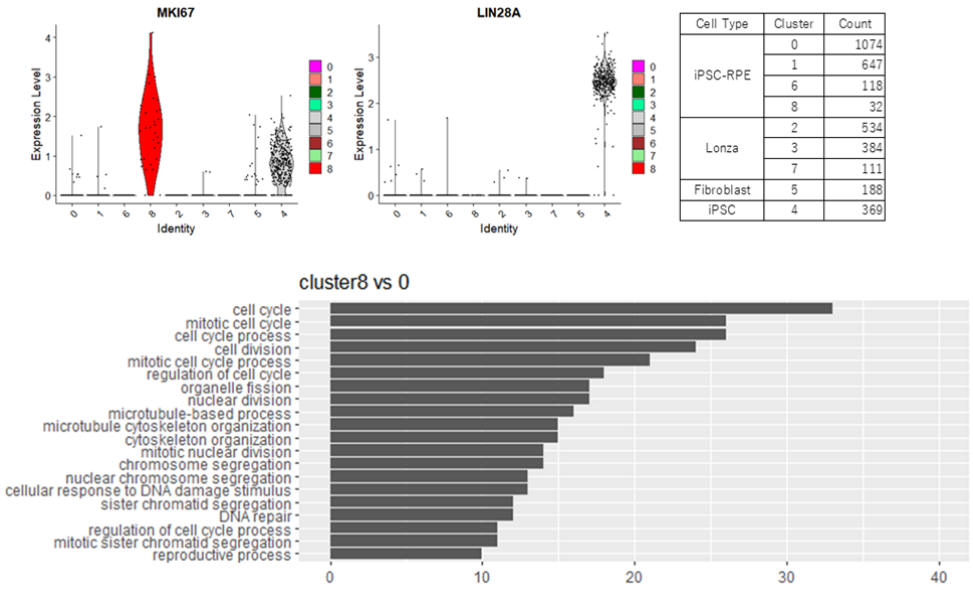

Cell Type	Cluster	Count
iPSC-RPE	0	1074
	1	647
	6	118
	8	32
Lonza	2	534
	3	384
	7	111
Fibroblast	5	188
iPSC	4	369

Figure 2 -figure supplement 3 A minor cluster of iPSC-RPE defined in **Figure 2B**, which consisted of 32 cells (*upper right*), showed a stem cell-like feature with higher expression of proliferation marker *MIK67* (*upper left*) and active cell cycle by gene enrichment analysis (*lower panel*), but was seemingly not a residual of undifferentiated iPSCs as shown by little expression of pluripotency marker *LIN28A* (*upper middle*).

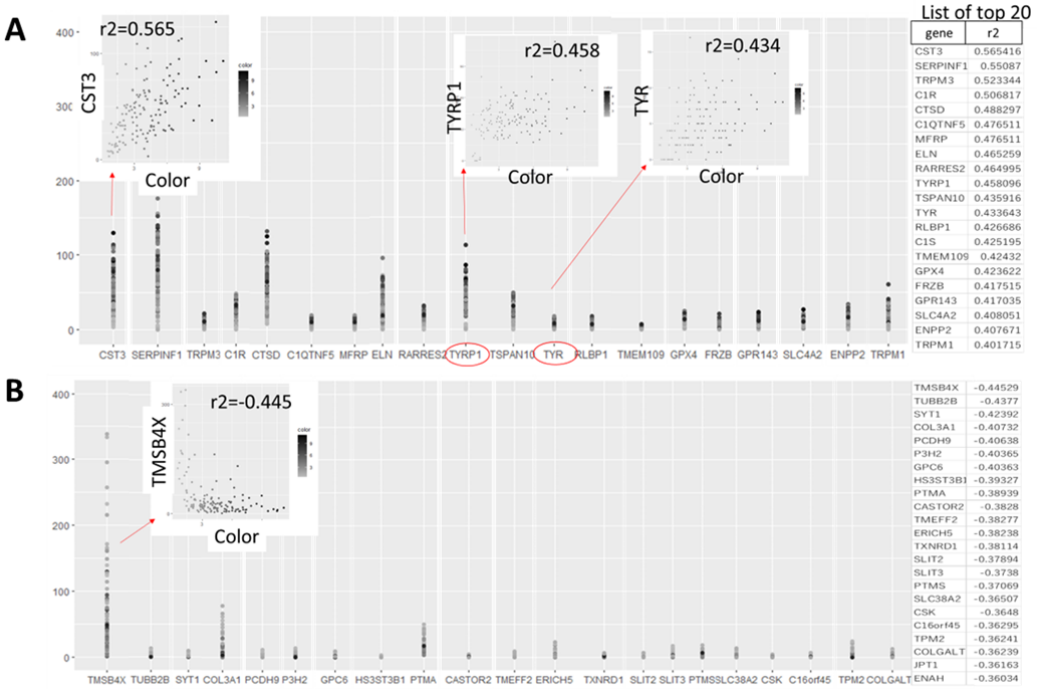

Figure 3 Correlation analysis between the expression level of each gene and the color of the iPSC-RPE.

List of the genes with positive (**A**) and negative (**B**) correlation to color intensities of *in vitro* cultured iPSC-RPE cells are shown. Even for the gene with the highest correlation to the color, the correlation value was 0.565. Notably, the melanin-synthesis enzymes *TYRP1* and tyrosinase (*TYR*) both showed only weak correlations (correlation value = 0.458 and 0.434, respectively).

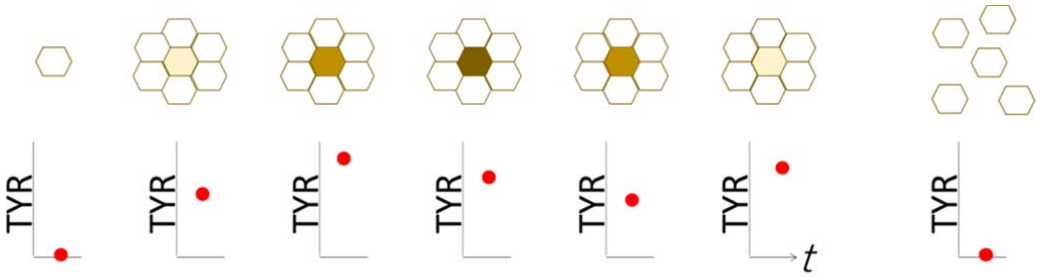

Figure 3 –figure supplement 1 Hypothetical model for the interpretation of weak correlation between the expression of *TYR* and the degree of pigmentation in iPSC-RPE cells.

When cultured *in vitro*, RPEs become more pigmented at higher cell-density, and return less pigmented when re-plated to lower cell density. The material of the color in RPE is melanin, which is synthesized by the enzymes such as TYRP1 and TYR, although the expressions of *TYRP1* and *TYR* were not strongly correlated with the color of RPE **(Figure 3A).**

The interpretation for this could be:

i) When RPEs contact each other, the nature as protective cell makes them to synthesize melanin, with upregulation of *TYRP1* and *TYR*.

ii) With sufficient amount of melanin, *TYRP1* and *TYP* become downregulated.

iii) Melanin will be divided among the daughter cells or secreted, which makes the cells less pigmented.

iv) When the amount of melanin becomes lower, *TYRP1* and *TYR* become upregulated again.

This model interprets the colors of iPSC-RPE cells are representing not a stable characteristic but a temporal condition of each cell, which makes it reasonable for the iPSC-RPE cells not having a specific gene expression profile that reflects on the degree of pigmentation (as shown in **Figure 2**).

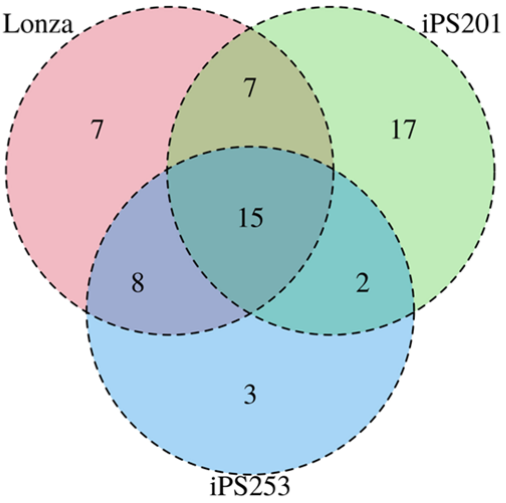

KEGG_LYSOSOME
KEGG_PROXIMAL_TUBULE_BICARBONATE_RECLAMATION
KEGG_PATHOGENIC_ESCHERICHIA_COLI_INFECTION
KEGG_SYSTEMIC_LUPUS_ERYTHEMATOSUS
KEGG_HYPERTROPHIC_CARDIOMYOPATHY_HCM
KEGG_ARRHYTHMOGENIC_RIGHT_VENTRICULAR_CARDIOMYOPATHY_ARVC
KEGG_DILATED_CARDIOMYOPATHY
KEGG_AXON_GUIDANCE
KEGG_FOCAL_ADHESION
KEGG_ECM_RECEPTOR_INTERACTION
KEGG_COMPLEMENT_AND_COAGULATION_CASCADES
KEGG_LEUKOCYTE_TRANSENDOTHELIAL_MIGRATION
KEGG_REGULATION_OF_ACTIN_CYTOSKELETON
KEGG_PATHWAYS_IN_CANCER
KEGG_SMALL_CELL_LUNG_CANCER

Figure 4 GSEA of iPSC-RPE cells elucidated gene sets correlated with color intensities. GSEA revealed 15 pathways that had high correlation with the intensities of the color of iPSC-RPE. Among them, there were lysosome-related and complement-related pathways.

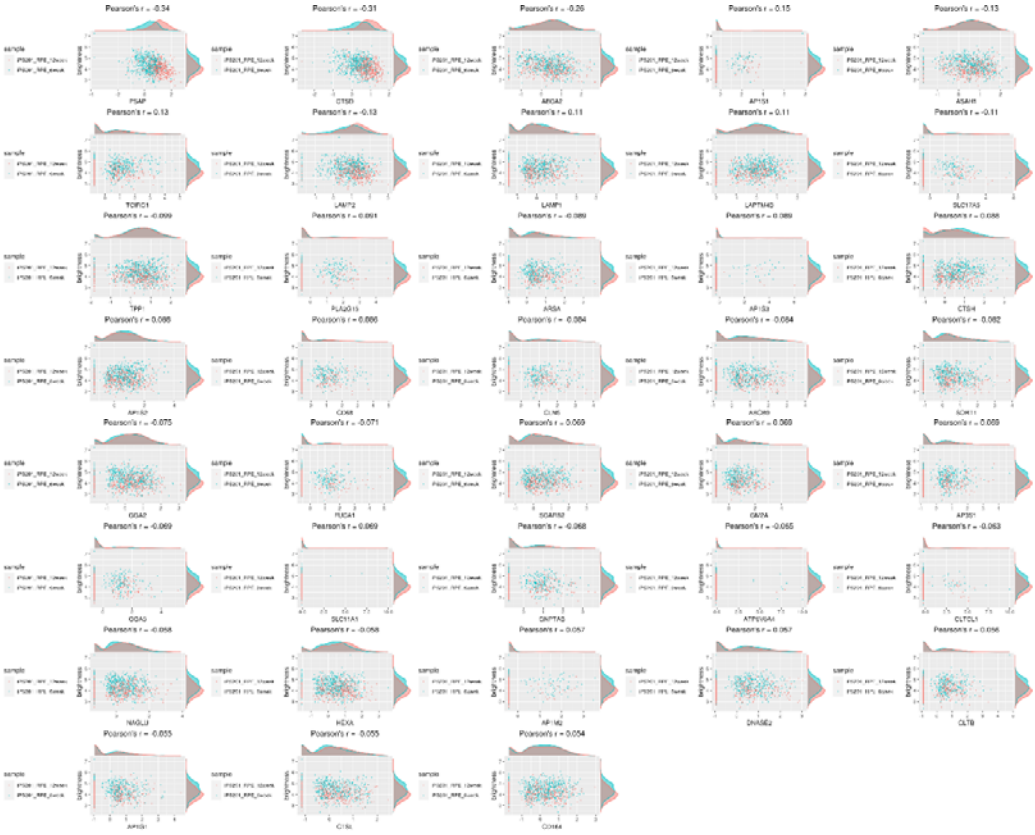

Figure 4 –figure supplement 1 Genes of lysosome-related pathway showed correlation with the color of iPSC-RPE cells.

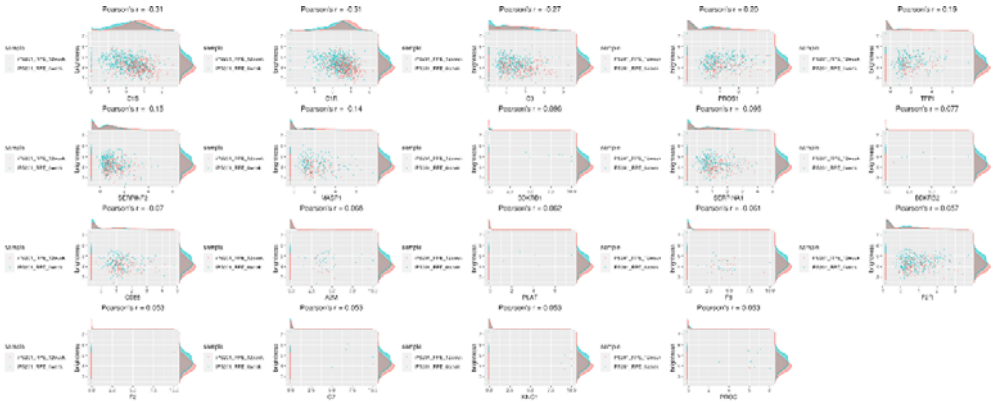

Figure 4 –figure supplement 2 Genes of complement-related pathway showed moderate correlation with the color of iPSC-RPE cells.

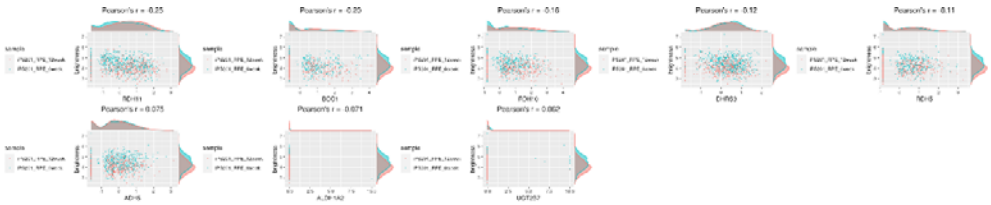

Figure 4 –figure supplement 3 Genes related to retinol metabolism had weak correlation with the color of iPSC-RPE cells.

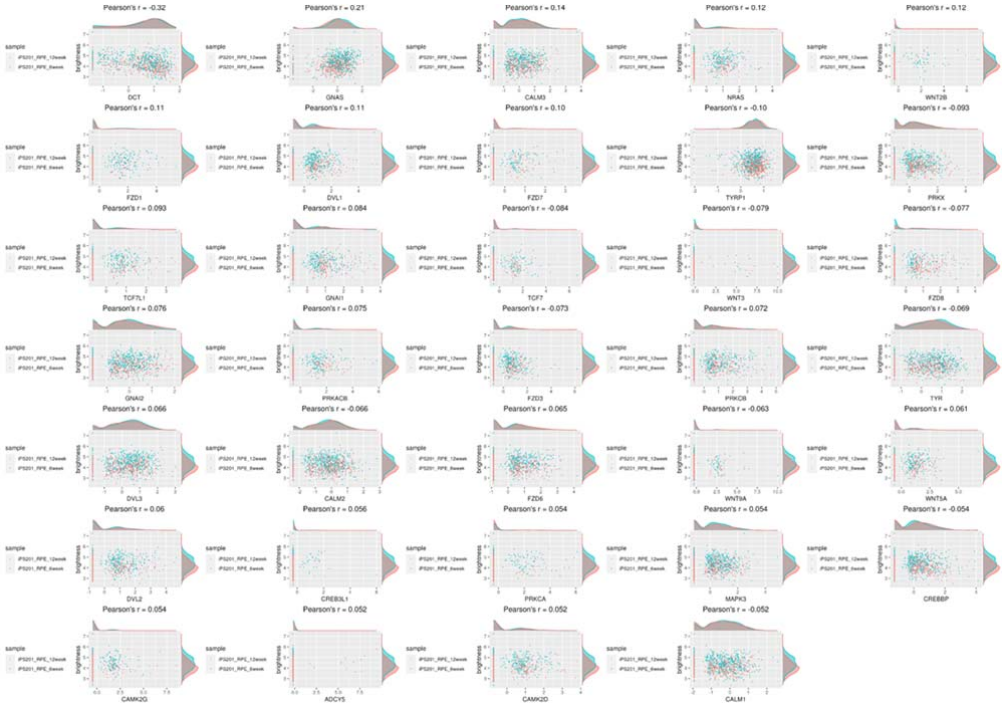

Figure 4 –figure supplement 4 Genes related to melanogenesis had weak correlation with the color of iPSC-RPE cells.